ACS APPLIED MATERIALS & INTERFACES

www.acsami.org
Research Article

Sonodynamic Therapy Induces Pyroptosis and Recruits CAR-NK Cells to Enhance the Treatment of Oral Squamous Cell Carcinoma

Jing Meng, Jiaxin Zuo, Luyu Li, Yunxuan Zhang, Minghao Zhao, and Ping Xiong*

Cite This: ACS Appl. Mater. Interfaces 2025, 17, 29352−29363
Read Online

ABSTRACT: **Background:** Immunotherapy strategies have demonstrated promising efficacy in treating various cancers. However, cancer cells often evade immune surveillance by reducing their immunogenicity, which limits immune cell infiltration into the tumor microenvironment. Pyroptosis, a proinflammatory form of programmed cell death, is characterized by the formation of plasma membrane pores that lead to the release of intracellular contents and stimulate a robust immune response. **Results:** To exploit this mechanism, we developed hematoporphyrin monomethyl ether (HMME)-loaded nanoliposomes capable of efficiently accumulating at the tumor site. Upon ultrasound irradiation, these nanomedicines generate reactive oxygen species (ROS) that activate Caspase-3, which cleaves Gasdermin E (GSDME) and induces tumor cell pyroptosis. Notably, this sonodynamic therapy (SDT) based on nanosonosensitizers enhanced the targeted enrichment of chimeric antigen receptor (CAR)-engineered natural killer (NK) cells at the ultrasound-irradiated tumor site, significantly improved the tumor immune response, and effectively inhibited the growth and proliferation of oral squamous cell carcinoma (OSCC) cells both in vivo and in vitro. **Conclusions:** Given that NK cell immunotherapy has an excellent safety profile with minimal risks of cytokine release syndrome and neurotoxicity, this approach holds promise as an adjunct to various NK cell-based immunotherapies through SDT-induced pyroptosis.

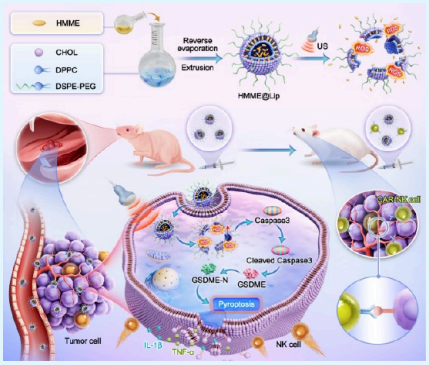

KEYWORDS: *sonodynamic therapy, pyroptosis, CAR-NK, cancer immunotherapy, oral squamous cell carcinoma*

1. INTRODUCTION

According to the American Cancer Society, head and neck squamous cell carcinoma (HNSCC) ranks as the eighth most common cancer globally and remains the leading cause of death among head and neck tumors.[1,2] Oral squamous cell carcinoma (OSCC) is the most prevalent cancer within this group, and its incidence has been steadily increasing. Clinically, treatment options for HNSCC, including OSCC, primarily involve surgery, often combined with traditional modalities such as radiotherapy, chemotherapy, or chemoradiotherapy. Traditional systemic chemotherapy and the use of cetuximab in treating recurrent cases are associated with significant long-term side effects, including drug toxicity. As a result, the five-year survival rate for these patients remains suboptimal,[3] underscoring the need for multidisciplinary treatment strategies to identify safer and more effective therapeutic alternatives.[4]

The combination of checkpoint blockade with emerging therapeutic strategies has demonstrated synergistic effects in cancer treatment, enhancing the immune-mediated cytotoxicity of $CD8^+$ T lymphocytes.[5] Unlike T cells, natural killer (NK) cells possess the unique ability to detect discrepancies in inhibitory signaling pathways in an antigen-independent manner.[6,7] This allows NK cells to distinguish malignant cells from healthy host cells, with a particular affinity for targeting and eliminating stem-like cancer cells, which exhibit increased tumorigenic potential and resistance to conventional therapies[8] Moreover, NK cell-based immunotherapy is characterized by a favorable safety profile, notably in the absence of severe complications such as cytokine release syndrome or graft-versus-host disease, as evidenced by clinical trials in various hematologic malignancies, including leukemia, lymphoma, and myeloma.[9,10] Despite these promising findings, the clinical application of NK cell-based therapies in solid tumors remains limited. For NK cells to exert effective antitumor activity, efficient recruitment and infiltration into the tumor microenvironment (TME) are essential.[11] However, the TME poses significant challenges, including a dense physical stromal barrier and disrupted chemokine gradients,[12,13] which hinder NK cell infiltration and, consequently, the overall efficacy of immunotherapy.[14] Identifying strategies to safely and effectively enhance NK cell infiltration into solid tumors

Received: February 20, 2025
Revised: April 27, 2025
Accepted: April 30, 2025
Published: May 8, 2025

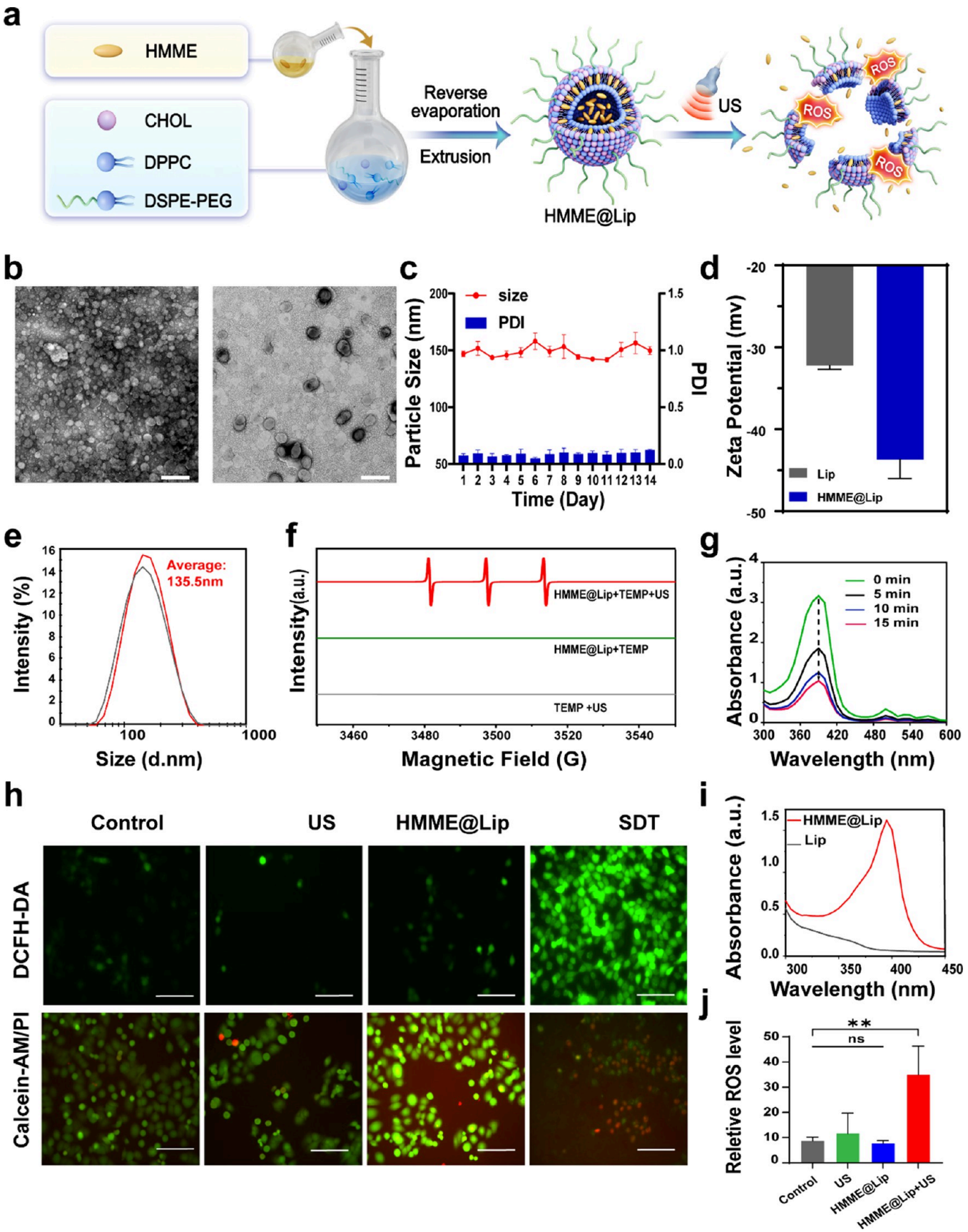

Figure 1. (a) Schematic illustration of the construction of HMME@Lip nanosonosensitizers and the US-triggered $^1O_2$ production assisted by HMME@Lip. (b) TEM image showed the quasi-spherical morphology of HMME@Lip with high dispersity (scale bar = 500 nm). (c) Time-dependent changes in particle size and PDI of HMME@Lip in PBS at 4 °C. (d) Zeta potential of liposomes (Lip) and HMME@Lip (n = 3). (e) Hydrodynamic diameters of HMME@Lip nanosonosensitizers in PBS, measured by DLS. (f) ESR spectra of HMME@Lip with or without US

https://doi.org/10.1021/acsami.5c03584
ACS Appl. Mater. Interfaces 2025, 17, 29352−29363

Figure 1. continued

treatment, indicating the generation of $^1O_2$. (g) Time-dependent DPBF absorption spectra in the presence of HMME@Lip under US irradiation for different durations. (h) CLSM images of CAL27 cells stained with DCFH-DA, Calcein-AM, and PI after various treatments: control (no treatment), US only, HMME@Lip only, and HMME@Lip combined with US irradiation (scale bar = 100 μm). (i) UV−vis absorption spectra of Lip and HMME@Lip, confirming the successful encapsulation of HMME into the liposome. (j) Corresponding semiquantitative analysis of relative ROS levels (n = 5). Statistical analysis was performed by one-way ANOVA. Data are presented as mean ± standard deviation (SD), with *p < 0.05, **p < 0.01, ***p < 0.001, and n.s.: no significant difference.

represents a critical and ongoing challenge for optimizing therapeutic outcomes.

Ultrasound (US) is one of the most widely recognized noninvasive physical irradiation techniques, playing a crucial role not only in clinical diagnosis but also in therapeutic applications.[15] Sonodynamic therapy (SDT), an emerging noninvasive treatment modality, offers several advantages, including high tissue penetration, nonionizing radiation, excellent controllability, and cost-effectiveness.[16] In the typical SDT process, US activates sonosensitizers, which subsequently generate reactive oxygen species (ROS) that induce cancer cell death through the apoptotic pathway.[17,18] Preclinical animal models have shown that the tumor cell debris resulting from SDT can serve as a source of tumor-associated antigens, triggering host immune responses that enhance antitumor immunity. However, apoptosis is often a "silent" cell death process, and cancer cells frequently develop resistance to apoptosis, which presents a significant challenge for achieving effective therapeutic outcomes.[19] In contrast to apoptosis, which typically does not provoke a strong immune response, inflammasome-driven pyroptosis has emerged as an alternative form of programmed cell death that induces potent immune activation. Pyroptosis is an inflammatory cell death process that activates the innate immune system. In tumor cells expressing gasdermin E (GSDME),[20] caspase-3 cleaves GSDME into two fragments: the C-terminal (GSDME-C) and the N-terminal (GSDME-N).[21] This cleavage converts the noninflammatory apoptotic process into an inflammatory pyroptotic response, thereby enhancing antitumor immunity. This transition from apoptosis to pyroptosis provides a promising strategy to improve the therapeutic efficacy of SDT by not only inducing cancer cell death but also triggering a robust immune response[22]

Inspired by the therapeutic properties of SDT and the immune response triggered by pyroptosis, we developed a combined therapeutic strategy that integrates SDT, pyroptosis induction in tumor cells, and CAR-NK cell therapy. This approach was successfully implemented using a nanoliposome platform loaded with an acoustic sensitizer. The key components of the nanosonosensitizer include FDA-approved drugs, such as liposomes to encapsulate therapeutic agents and hematoporphyrin monomethyl ether (HMME) as an ultrasound-responsive sonosensitizer.[5] Upon US stimulation, ROS are generated, which induce GSDME-dependent pyroptosis in tumor cells, release proinflammatory cytokines, recruit NK cells, trigger a systemic immune response, and facilitate tumor cell death, while also inhibiting distant metastasis. The antitumor effects of pyroptosis, mediated by ROS generation and the Caspase-3/GSDME pathway, were thoroughly validated through RNA sequencing, morphological analysis, and Western blotting. Notably, in a severe immunodeficiency mouse (NSG) model, the combined adoptive transfer of CAR-NK cells led to a significant accumulation of CAR-NK cells at the orthotopic tumor site, greatly enhancing the efficacy of CAR-NK immunotherapy. These promising results offer new avenues for improving CAR-NK-based targeted therapy for solid tumors via the integration of SDT.

2. RESULTS AND DISCUSSION

2.1. Design, Synthesis, and Characterization of HMME@Lip. The synthesis of the nanosonosensitizer HMME@Lip is illustrated in Figure 1a. A highly biocompatible liposome was selected as the nanoplatform for encapsulating the sonosensitizer HMME using a reverse evaporation method. The resulting HMME-loaded liposomes (HMME@Lip) were then homogenized by high-pressure nitrogen extrusion, followed by ultracentrifugation filtration to remove any free drug and ensure the purity of the formulation.[5]

As shown in Figure 1b, the transmission electron microscopy (TEM) image revealed that HMME@Lip exhibited a monodispersed, uniform particle morphology. Long-term monitoring (14 days) demonstrated the good structural stability of HMME@Lip under physiological conditions, with minimal changes in particle size and a low polydispersity index (PDI) (Figure 1c). The rigidity of the lipid membrane contributed to its stability. The average hydrodynamic diameter of the nanosonosensitizer was approximately 135.5 nm, as measured by a Malvern laser particle size analyzer, and the surface Zeta potential was −43.7 mV, indicating strong electrostatic repulsion, which prevented aggregation and enhanced stability (Figure 1d,e). Electron spin resonance (ESR) and 1, 3-diphenylisobenzofuran (DPBF) assays (Figure 1g) were employed to qualitatively and quantitatively assess ROS generation. It was found that singlet oxygen ($^1O_2$) was generated by HMME@Lip under US irradiation, as evidenced by the characteristic ESR peak. When coincubated with CAL27 cells, the DCFH-DA probe emitted intense green fluorescence upon US excitation, confirming ROS production (Figure 1j). The UV−vis absorption spectrum of HMME@Lip displayed a distinct absorption peak around 398 nm (Figure 1i), confirming the successful encapsulation of HMME into the nanoparticles. The encapsulation efficiency and drug loading of the liposomes measured according to the standard curve were 38.3 and 6.5%, respectively. To evaluate the cell viability and toxicity of HMME@Lip, CCK-8 assays were performed on CAL27 cells coincubated with varying concentrations of HMME@Lip under US excitation. Representative inverted fluorescence images demonstrated the significant toxicity of HMME@Lip to tumor cells upon US stimulation (Figures 1h and S1). In contrast, in the absence of US stimulation, HMME@Lip exhibited excellent biological safety. These findings supported the potential of SDT-based tumor treatment.

2.2. RNA Sequencing. When CAL27 cells were incubated with HMME@Lip and stimulated with US, we observed cell membrane blebbing and protrusion under the microscope, which were characteristic features of pyroptosis (Figure 3b). However, previous studies have indicated that SDT typically

https://doi.org/10.1021/acsami.5c03584
ACS Appl. Mater. Interfaces 2025, 17, 29352−29363

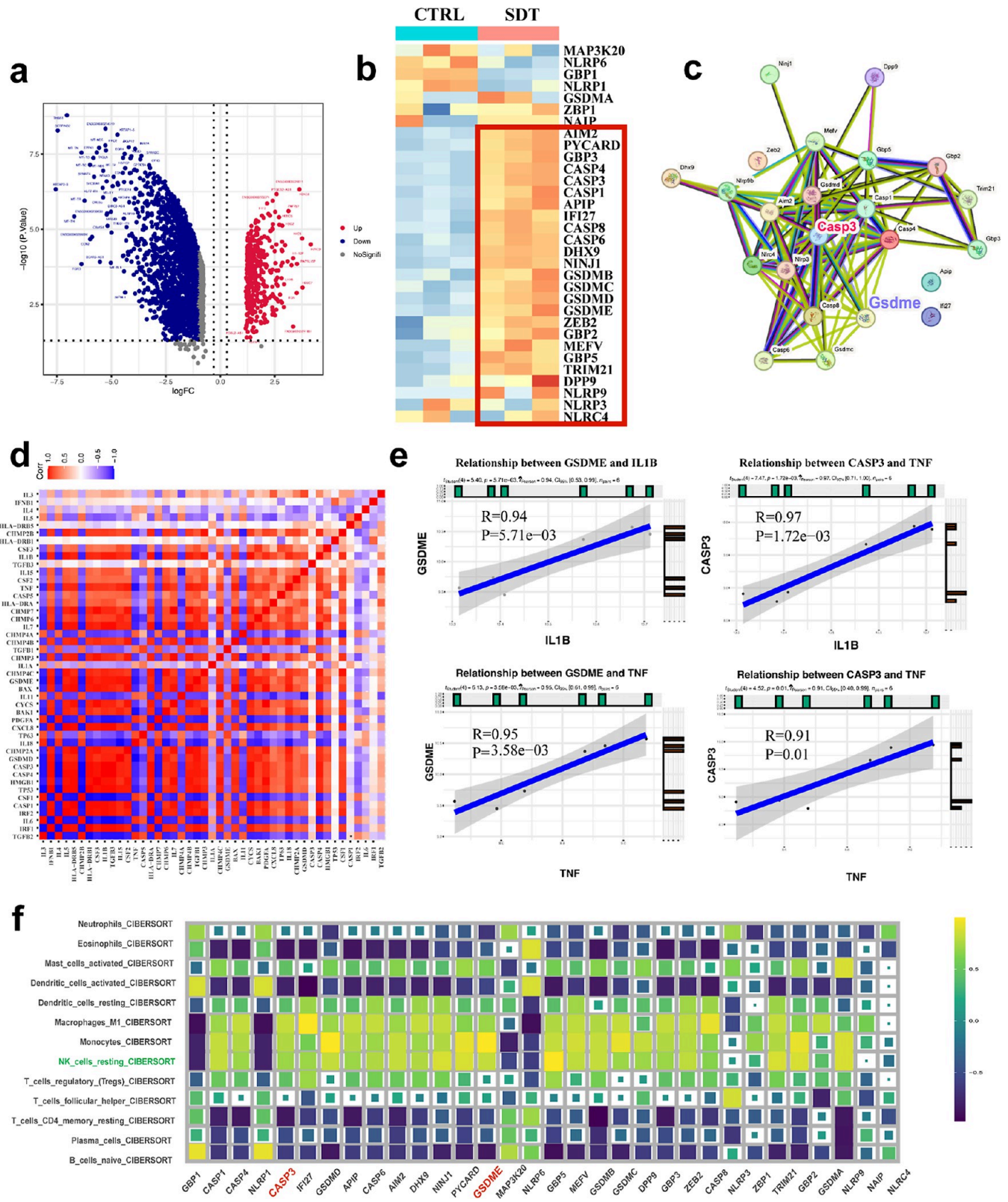

Figure 2. RNA sequencing of CAL27 cells after different treatments. (a) Volcano plot of DEGs from transcriptome sequencing in the CTRL and SDT groups. (b) Expression levels of pyroptosis-related genes in the CTRL and SDT groups. (c) Multiple-protein interaction analysis of pyroptosis-related protein in the CTRL and SDT groups. (d) Correlation analysis of pyroptosis-related genes in the CTRL and SDT groups. (e) Correlation analysis between GSDME and CASP3 with IL1B and TNF. (f) Immune infiltration analysis of pyroptosis-related genes in the CTRL and SDT groups.

induces apoptosis in tumor cells. To further investigate the potential therapeutic mechanism of HMME@Lip on OSCC cells, we conducted additional experiments on CAL27 cells. Unsupervised hierarchical clustering of the RNA-sequencing

https://doi.org/10.1021/acsami.5c03584
ACS Appl. Mater. Interfaces 2025, 17, 29352−29363

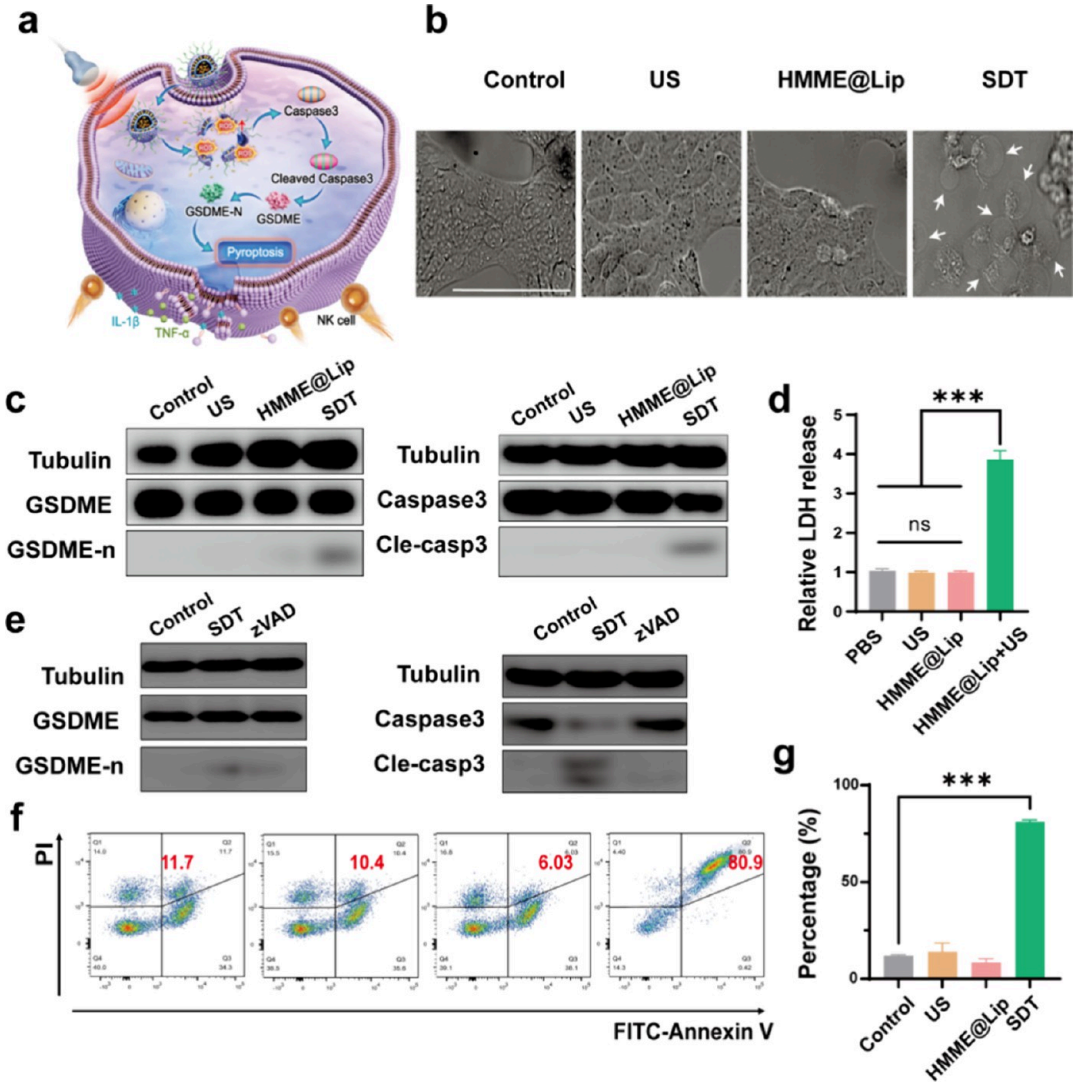

Figure 3. (a) Pyroptosis induced by the SDT strategy. (b) Bright-field CLSM images of CAL27 cells following different treatments. The white arrows indicate bubble-like protrusions on the surface of the cell membrane (scale bar = 100 μm). (c,e) Western immunoblot analysis of the expression levels of pyroptosis-related proteins (Caspase-3, cleaved-Caspase-3, GSDME, and GSDME-n) in CAL27 cells after different treatments. (d) Release of LDH from CAL27 cells after different treatments (n = 3). (f) Annexin V-FITC and PI staining assays. (g) Corresponding semiquantitative analysis of CAL27 cells after different treatments. Statistical analysis was conducted using one-way ANOVA. Data were presented as mean ± SD, with $^{*}p < 0.05$, $^{**}p < 0.01$, $^{***}p < 0.001$, and n.s. indicating no significant difference.

data revealed clear clustering of samples within the same treatment groups, indicating the high reliability of the data (Figure S2a). A total of 2811 differentially expressed genes (DEGs) were identified between the SDT and CTRL groups. Among these, 400 genes (14.23%) were downregulated, while 2411 genes (85.77%) were upregulated (Figure S2b).

To further investigate the molecular biological differences between the CTRL and SDT groups and their relationship with pyroptosis, we performed transcriptome sequencing analysis (Figure 2a) and screened for differential expression of pyroptosis-related genes. The results revealed that under SDT treatment, several pyroptosis-related genes were upregulated (Figure 2b). Protein−protein interaction analysis of these upregulated genes using STRING revealed that Casp3 and GSDME play central roles in the interaction network (Figure 2c). Further analysis of interacting proteins showed that GSDME had a correlation coefficient of 0.94 with IL1B (P < 0.01, Figure 2e) and a correlation coefficient of 0.95 with TNF (P < 0.01, Figure 2e). CASP3 showed a correlation coefficient of 0.97 with IL1B (P < 0.01, Figure 2e) and a correlation coefficient of 0.91 with TNF (P = 0.01, Figure 2e). These results suggested that pyroptosis, as an inflammatory form of cell death (Figure 2d), leads to the release of inflammatory factors that can enhance the TME..

Additionally, to explore whether pyroptosis is involved in inflammatory responses and immune activation, we conducted an immune infiltration analysis. The results showed that GSDME or CASP3 was significantly positively correlated with resting NK cell infiltration (Figure 2f).[20] Therefore, to enhance NK cell infiltration and boost the immune system's attack on the tumor through SDT, one approach may be the exogenous infusion of NK cells, preactivated with cytokines such as IL-2 to improve their killing ability.[23]

2.3. HMME@Lip Induce Pyroptosis of CAL27 Cells. Pyroptosis is characterized by inflammation and is closely associated with the Gasdermin family of proteins, which includes Gasdermin A, B, C, D, E, and DFNB59.[24,25] To investigate whether SDT induces pyroptosis in cancer cells, we

https://doi.org/10.1021/acsami.5c03584
ACS Appl. Mater. Interfaces 2025, 17, 29352−29363

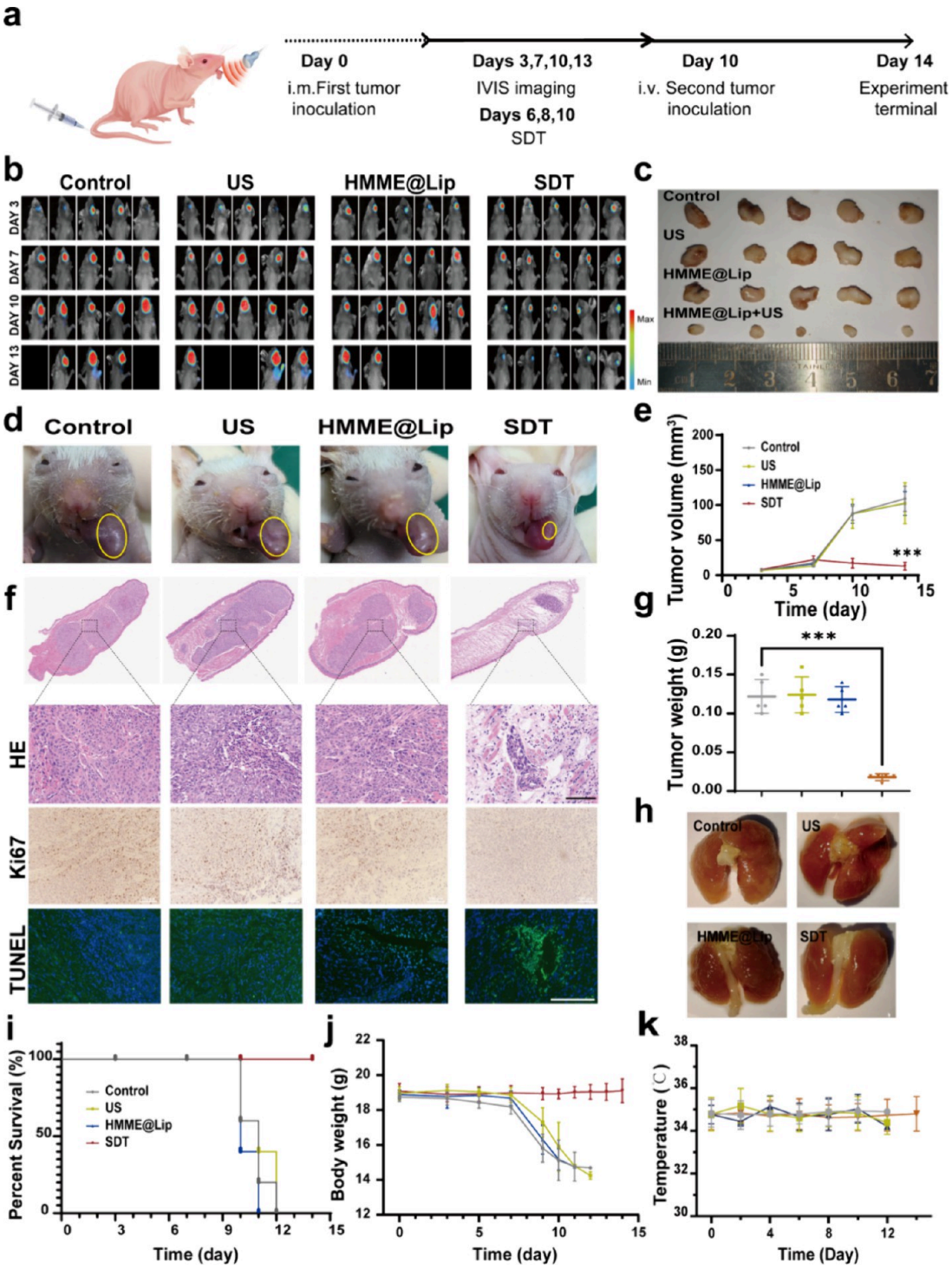

Figure 4. (a) Treatment schedule for various modalities based on SDT. (b) In vivo imaging was used to track the spread and growth of luc-CAL27 tumor cells injected into mice after different treatments. (c) Photographs of the primary tumors. (d) Photographs of tumor-bearing mice and tumor regions at the end point of the experiment. (e) Tumor growth curves of orthotopic tumor-bearing mice following various treatments were shown in the figure, $n = 5$. (f) Digital images and H&E staining, TUNEL assay, and *Ki67* immunofluorescence staining of tumor regions from orthotopic tumor-bearing mice 14 days post-treatment. Scale bars: 100 μm (H&E, *Ki67*) or 50 μm (TUNEL). (g) Weight of dissected tumors from different treatment groups after 14 days. (h) Representative photographs showing the gross appearance of tumor nodules in the lungs were presented. (i) Survival curves of mice treated with different modalities. (j,k) Curves of body weight and body temperature of mice from different treatment groups. Statistical significance was calculated using Student's *t* test: $*p < 0.05$, $**p < 0.01$, $***p < 0.001$, and n.s. for nonsignificant.

examined the morphological changes in CAL27 cells after SDT treatment. Typical pyroptotic features, including membrane blebbing and protrusion, were observed (Figures 3b and S3). Since some nanomaterials have been shown to induce pyroptosis through the Caspase-3-GSDME pathway,[26] we assessed the expression of GSDME-n through Western blotting. After SDT, we detected the expression of cleaved-Caspase-3 and GSDME-n (Figures 3c and S4). This process

https://doi.org/10.1021/acsami.5c03584
ACS Appl. Mater. Interfaces 2025, 17, 29352−29363

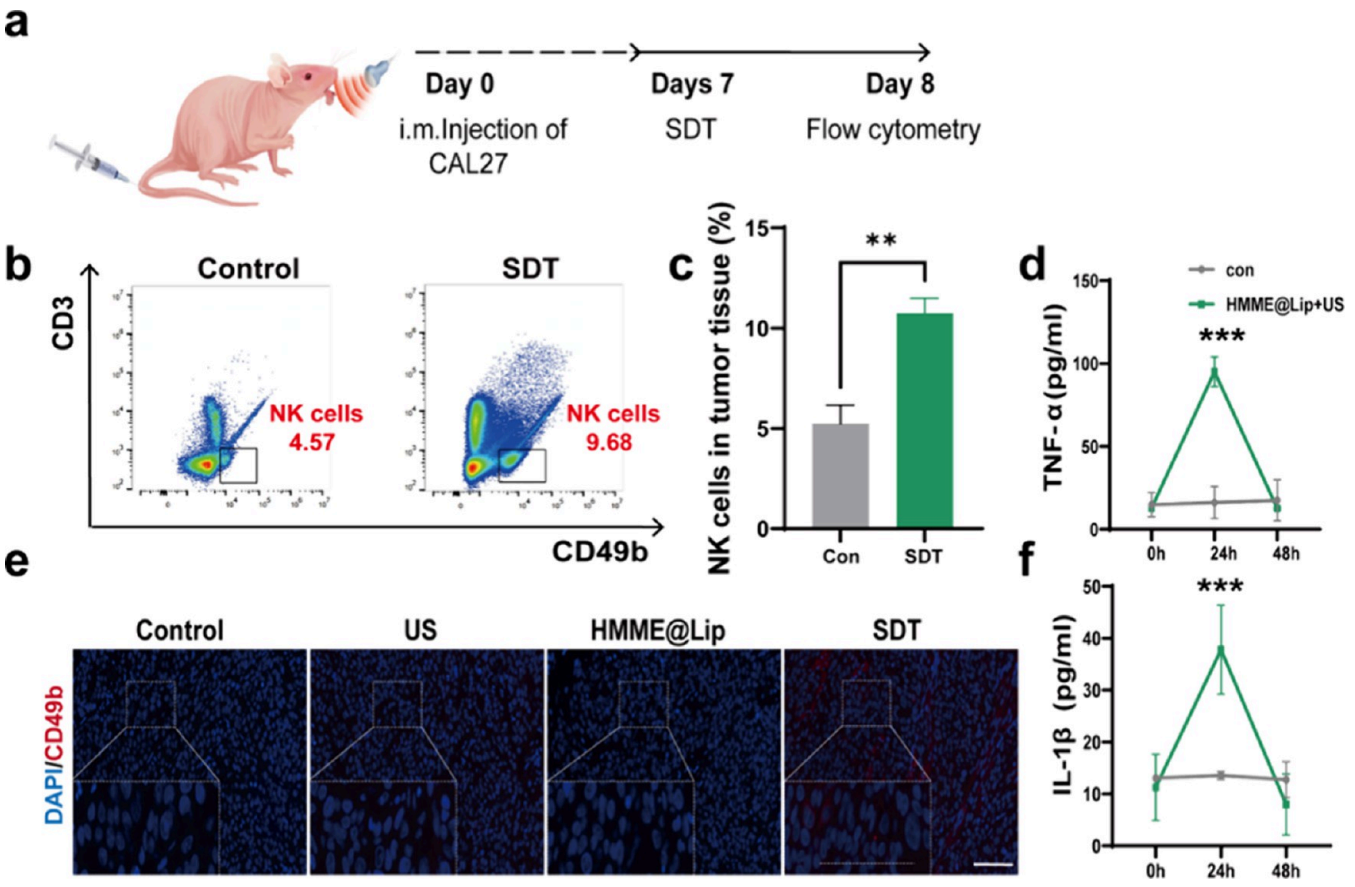

Figure 5. (a) Treatment schedule for modalities based on SDT. (b,c) Representative flow cytometry plots showing tumor-infiltrating NK cells and quantitative statistical analysis. (d) Cytokine levels of TNF-α in sera from mice collected at 0−48 h after HMME@Lip-augmented SDT treatment. (e) Representative immunofluorescence images showing NK cell recruitment following SDT treatment were represented. (scale bar = 100 μm). (f) Cytokine levels of IL-1β in sera from mice collected at 0−48 h after HMME@Lip-augmented SDT treatment. Statistical significance was calculated using Student's t test: $^{*}p < 0.05$, $^{**}p < 0.01$, $^{***}p < 0.001$.

was reversed by the pyroptosis inhibitor zVAD, suggesting that GSDME is essential for SDT-induced pyroptosis in oral squamous cell carcinoma cells (Figure 3e). The rapid formation of Gasdermin pores led to cell swelling, followed by membrane rupture and the release of intracellular contents, including inflammatory cytokines. This was reflected in the elevated extracellular lactate dehydrogenase (LDH) levels in the SDT group (Figure 3d). We further investigated pyroptosis in CAL27 cells using flow cytometric assays after different treatments (Figure 3f,g). The ratios of pyroptosis cells in the SDT groups were significantly higher than in the other three groups, with pyroptosis cell populations reaching 80.9%. In addition, we observed morphological changes in cancer cells after SDT treatment across several other cell lines (Figure S5). Notably, SDT induced membrane blebbing in a variety of cancer cells, including the 4T1 cell line,[22] which has low GSDME expression. This suggested that SDT can induce pyroptosis in cancer cells in a GSDME-independent manner.[27] Given that some nanomaterials can cleave GSDMD to release GSDMD-n,[28] we evaluated the production of GSDMD-n during SDT, and the results suggested that GSDMD may be involved in another pathway of GSDME-independent pyroptosis (Figure S6). Furthermore, this GSDME-independent pyroptosis may be attributed to the acoustic cavitation effect of US. As a mechanical wave, US can induce the nucleation, growth, or oscillation of microbubbles within tissue fluids. When these microbubbles burst, the resulting shock wave generates a large pressure gradient over a short period, causing direct physical damage to the tumor. In this process, nanoparticles can provide nucleation sites for bubble formation, further enhancing the SDT effect.[29]

2.4. In Vivo Antitumor Effect. Due to the excellent pyroptosis-inducing effect of HMME@Lip on a variety of malignant tumor cells in vitro, we further investigated its in vivo tumor-suppressive effect using orthotopic Cal27 tumor-bearing BALB/c mice. Initially, evaluating the in vivo biosafety of the nanosonosensitizer is a critical prerequisite to ensure the safety of subsequent experiments. Healthy male C57 mice were randomly divided into a control group and an HMME@Lip group (5 mg/kg, single dose, intravenous injection). Biocompatibility was assessed through blood biochemistry and hematoxylin-eosin (H&E) histological examination of major organs. Statistical analysis of hematological data and liver and renal function assessments between the control and treated groups revealed no abnormalities in any of the physiological function indicators tested (Figure S7). H&E staining of the major organs from mice in each group showed no significant organ damage (Figure S8), suggesting that systemic side effects in the treated mice were negligible.

Subsequently, we evaluated the antitumor effects of SDT in CAL27 tumor-bearing nude mice. Three days after inoculating CAL27-Luc cells into the tongues of mice, 20 male mice with tumor volumes of approximately 19 mm^3 were selected and randomly divided into four groups (n = 5): (1) PBS group, (2)

https://doi.org/10.1021/acsami.5c03584
ACS Appl. Mater. Interfaces 2025, 17, 29352−29363

US group, (3) HMME@Lip group (intravenous injection), and (4) SDT group (HMME@Lip + US). Body weight and body temperature were measured every 2 days, or daily as appropriate, and tumor volume was measured after each in vivo imaging, with no significant differences in body temperature observed among the groups (Figure 4k). On day 7, all groups except the SDT group showed a significant decrease in average body weight (Figure 4j). This weight loss was attributed to the rapid tumor growth, which occupied the oral space and impaired the mice' ability to eat and drink. In contrast, SDT treatment significantly inhibited tumor growth, and the SDT group mice experienced a slight weight gain (Figure 4b−e). In vivo imaging showed progressive tumor growth over time and treatment, with the SDT group demonstrating near-complete tumor elimination by the end of the observation period, consistent with the results of the final tumor dissection (Figure 4c). To further assess the immune memory effect of SDT, CAL27 cells were reinoculated into the tail vein on day 10 to establish a lung metastasis model. The second inoculation led to continued weight loss in all groups except the SDT group, despite the slower tumor growth due to the spatial constraints in the oral cavity (Figure 4e,i,j). At the end of the study, the mice were euthanized due to severe weight loss (>20%). Gross anatomical images of the lungs showed reduced pulmonary nodules in the SDT group, and H&E staining confirmed fewer nodules in the lungs of the SDT-treated mice (Figure S9), indicating that SDT induced a long-lasting immune memory effect.

To further confirm the anticancer effect of SDT, we performed Ki67 and TUNEL staining on tumor tissue sections. As anticipated, US irradiation or HMME@Lip injection alone did not significantly affect Ki67 expression, suggesting minimal impact on tumor proliferation. In contrast, Ki67 expression was nearly absent in the SDT group (Figure S10), indicating a potent inhibitory effect on tumor cell proliferation. Additionally, the antitumor efficacy of SDT was further corroborated by the presence of a fluorescent green signal localized to the nucleus in TUNEL-stained images (Figure 4f), suggesting significant induction of tumor cell apoptosis.

2.5. Activation of the Immune System by SDT. Based on the significant role of NK cells in solid tumors, we evaluated the effect of SDT on NK cell recruitment in vivo using nude mice. Representative inverted fluorescence images (Figure 5e) showed that $CD49b^+$ NK cells were not observed in the control, US, or HMME@Lip groups. However, NK cell infiltration was observed in the immunofluorescence images of the SDT group (Figure S11). To quantify NK cell recruitment and assess the reduction in tumor cells, we analyzed tumor tissues from mice euthanized on day 8 ($n = 6$) (Figure 5a). Flow cytometry results (Figure 5b,c) showed that the percentage of NK cells in the tumor site of the SDT group increased from 4.57% in the control group to 9.68%.

Following the demonstration of SDT's efficacy in tumor treatment and NK cell recruitment in vivo, we subsequently investigated its association with the activation of pyroptosis. Previous correlation analyses between pyroptosis-related proteins, including GSDME and Caspase-3, and inflammatory cytokines TNF-α and IL-1β, guided our focus on evaluating the changes in TNF-α and IL-1β levels in the serum of CAL27 tumor-bearing mice following SDT treatment. IL-1β is also a potent proinflammatory regulator for neutrophil recruitment, macrophage activation, and T-cell expansion. The results showed that, after 1 day of SDT, there was a significant increase in the secretion of proinflammatory cytokines, which likely contributed to the activation of antitumor immune responses and the recruitment of immune cells. However, the levels of TNF-α and IL-1β rapidly declined to near baseline through 48 h post-SDT treatment, indicating that the inflammation induced by SDT was an acute response without inducing a cytokine storm-like phenomenon. Furthermore, the elevated expression of GSDME-N and inflammatory cell infiltration induced by SDT (Figures S12 and S13) further confirmed the occurrence of pyroptosis during cancer cell death in vivo.

2.6. SDT Recruits CAR-NK Cells To Synergistically Inhibit Tumor Growth. An increasing number of researchers have suggested that NK cells, either autologous or allogeneic, may be more suitable than T cells for targeted cancer therapy.[7] Additionally, the availability of expanding NK cell lines offers a potentially unlimited source of effector cells for genetic engineering studies, with NK-92 cells being the most extensively studied and already reaching clinical trial stages.[30] In this context, CAR-engineered NK-92 cells could serve as a cost-effective and efficient alternative to primary CAR-NK or T cells.[13] OSCC expresses various tumor-associated antigens, which can be targeted for immune intervention. Among these, the epidermal growth factor receptor (EGFR) is particularly notable,[31] as its expression level distinguishes between normal and cancerous epithelial tissues and correlates with the malignancy grade. Furthermore, the EGFR is upregulated in a variety of solid tumors, making it a widely studied and promising target for cancer immunotherapy.[32]

To investigate how SDT-induced recruitment of immune cells influences CAR-NK cell activity, we constructed a second-generation EGFR-targeting CAR in a lentiviral vector backbone. This construct included a CD8α signal peptide (SP), a heavy-chain variable region (VH), a linker, a light-chain variable region (VL), an IgG1 Fc hinge, CD28 transmembrane and intracellular domains, and a CD3ζ signaling domain. The VH and VL sequences were derived from the commercial antibody cetuximab (Figures S14 and S15).[33,34] Redirecting NK-92 cells with an EGFR-specific CAR significantly enhanced their ability to target tumors (Figure S15b). We performed flow cytometry using an anti-$F(ab')^2$ antibody, which recognizes the scFv region of anti-EGFR.[35] The data in Figure S15d show that EGFR-CAR expression was significantly higher on EGFR-CAR-transfected NK-92 cells compared to primary NK-92 cells, which showed undetectable levels of EGFR-CAR.

In vitro, we measured the luminescence intensity of CAL27-Luc cells and observed that gene-edited CAR-NK-92 cells were significantly more efficient at lysing CAL27 cells compared to parental NK-92 cells (Figure S15c). One mechanism by which NK cells kill tumor cells is through the secretion of granzyme B (GzmB),[36] which can cleave GSDME and activate pyroptosis,[37] further enhancing antitumor immune responses and inhibiting tumor growth. This process may also synergize with the pyroptosis activation induced by SDT. To assess whether the enhanced cytolytic activity of CAR-NK cells was associated with increased GzmB secretion,[38] we cocultured EGFR-CAR-NK-92 cells with CAL27 cells at various E/T ratios for 24 h and measured GzmB production by ELISA. As shown in Figure S16, NK-92 cells produced low levels of GzmB, whereas CAR-NK cells secreted significantly more GzmB at each E/T ratio. These findings are consistent with the cytotoxicity data and collectively indicate that EGFR-CAR modification significantly enhances the effector function of NK cells against

https://doi.org/10.1021/acsami.5c03584
ACS Appl. Mater. Interfaces 2025, 17, 29352−29363

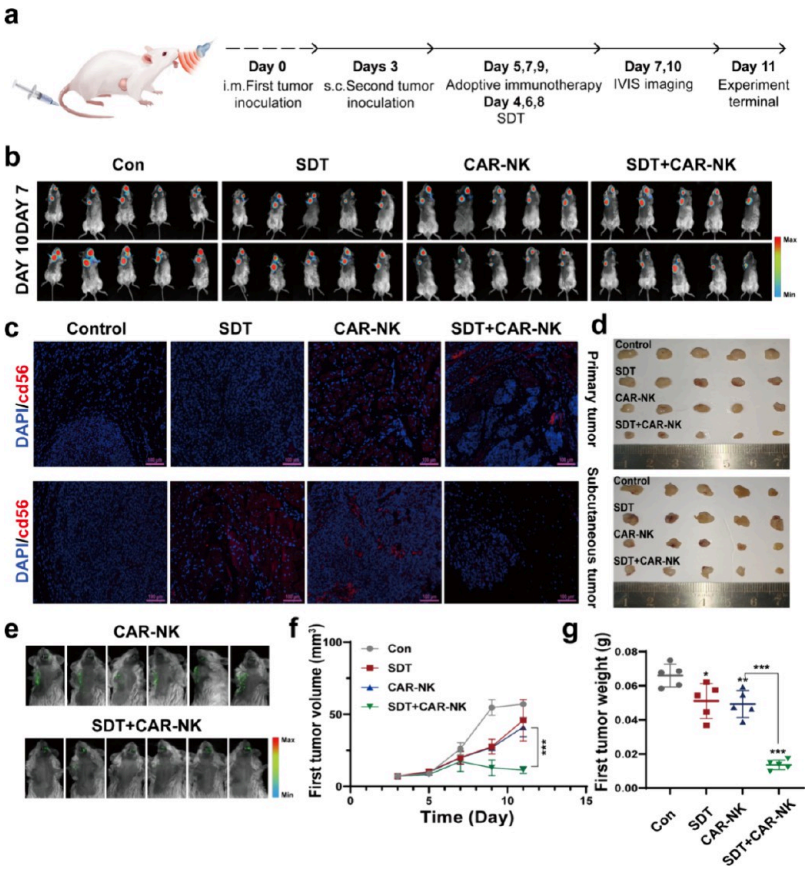

Figure 6. (a) Schematic representation of the treatment protocol and treatment duration in NSG mice for the ex vivo analysis. (b) In vivo bioluminescence imaging tracking the spread and growth of Luc-CAL27 tumor cells in mice following different treatments (n = 5). (c) Representative immunofluorescence images illustrated the infiltration of CAR-NK cells in both primary and distant subcutaneous tumors after various treatments (scale bar = 100 μm, n = 5). (d) Photographs of primary and distant tumors post-treatment (n = 5). (e) In vivo imaging revealed targeted enrichment of Zsgreen labeled CAR-NK cells in NSG mice (n = 6). (f) Tumor growth curves for different groups of orthotopic tumor-bearing mice after various treatments were indicated in the figure. (Error bars represent SD, n = 5). (g) Weight of dissected primary tumors from different treatment groups after 12 days of treatment (n = 5). Statistical significance was determined using Student's t test: *p < 0.05, **p < 0.01, ***p < 0.001, and n.s. for nonsignificant differences.

CAL27 cells. Besides, we next simulated the effect of SDT on the recruitment of CAR-NK cells using an in vitro transwell model (Figure S15e). The quantitative analysis results of the lower compartment cells by flow cytometry showed (Figure S15f,g) that compared with the other three groups, the SDT group greatly increased the number of CAR-NK cell migration, which encouraged us to further investigate the recruitment of SDT to exogenously infused NK cells in vivo.

We established orthotopic OSCC and right axillary-stimulated metastatic tumor models in NSG mice. The experimental procedure is shown in Figure 6a. Three days after the initial CAL27-Luc tumor was inoculated into the orthotopic tongue, a second tumor was subcutaneously implanted in the right axillary region to simulate metastasis. In vivo imaging was then employed to monitor the biodistribution of HMME@Lip at specific time points (Figure S17). Twenty-four h after intratumoral injection, mice were euthanized. The results indicate that HMME@Lip efficiently accumulated in both primary and distant tumors within 2 h after injection, likely due to its prolonged blood circulation and high stability, which favor the EPR effect. Ex vivo imaging further showed that HMME@Lip was still retained at the tumor site after 24 h, providing a sufficient therapeutic window for US-mediated treatment of malignant tumors. These findings suggested that the prepared HMME@Lip formulation is biocompatible and holds promise for further in vivo therapies and clinical translation.

Tumor-bearing mice were irradiated with US immediately following each intravenous injection of the nanosonosensitizer, and CAR-NK cells were injected intravenously on the second day post-SDT. The treatment timeline is outlined in Figure 6a. The treatment outcomes for primary and mock distal tumors across different experimental groups are summarized in Figure 6f,g and Figure S18. CAR-NK cell therapy alone exhibited inhibitory effects on both primary and distal tumors. However, the growth of tongue tumors was gradually constrained by the limited oral space, leading to poor blood supply, which hindered CAR-NK cell enrichment in the tumor compared to subcutaneous tumors. The in vivo imaging data also showed a more pronounced signal in the subcutaneous tumor (Figure 6e), a hypothesis supported by immunofluorescence analysis showing positive CD56 expression (Figure 6c). SDT alone had a modest inhibitory effect on the growth of the primary tumor, likely due to the severe immunodeficiency of NSG mice, which limited the immune activation or vaccine-like effects of SDT. As a result, its efficacy was reduced, with tumor cell elimination primarily due to physical destruction rather than immune-mediated effects, leading to minimal impact on distant

https://doi.org/10.1021/acsami.5c03584
ACS Appl. Mater. Interfaces 2025, 17, 29352−29363

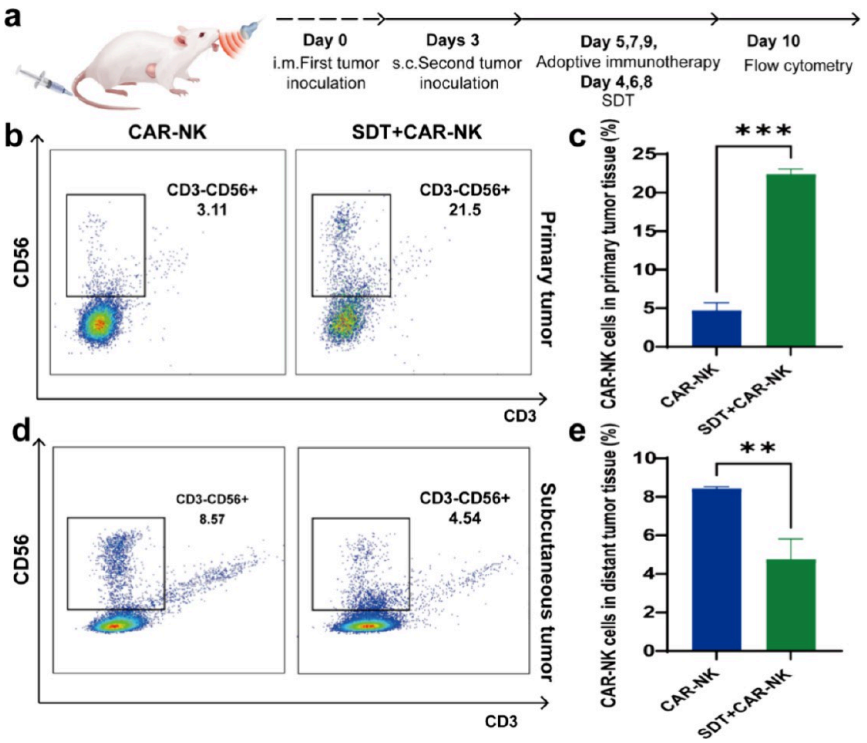

Figure 7. (a) Schematic representation of the treatment protocol and treatment duration in NSG mice for the ex vivo analysis. (b,c) Representative flow cytometry plots showed CAR-NK cell infiltration in primary tumors, along with corresponding quantitative analysis results (n = 6). (d,e) Representative flow cytometry plots showed CAR-NK cell infiltration in distant tumors, with corresponding quantitative analysis results (n = 6). Statistical significance was calculated using Student's t test: *p < 0.05, **p < 0.01, ***p < 0.001, and n.s. indicates nonsignificant differences.

metastatic tumors (Figure 6d–f). Notably, the combination of SDT and CAR-NK cells almost completely eradicated the primary tumor and significantly enhanced CAR-NK cell infiltration into the primary tumor (Figure 6c). Additionally, SDT's recruitment effect on CAR-NK cells potentially induced a "competition" between the primary tumor and distant metastatic tumors. While the primary tumor responded better to the treatment, the volume of distant metastatic tumors increased (Figure S18a,b), likely due to a reduced infiltration of CAR-NK cells in the metastatic sites, as shown in Figure 6e, the fluorescence signal in the tongue was enhanced, and the subcutaneous signal was weakened in the SDT combined with the CAR-NK group. NK cells can easily reach hematopoietic tumors in peripheral blood; however, infiltrating solid tumors is more challenging due to several biological barriers. To reach the solid tumor bed, NK cells must first extravasate from the blood, traverse the tumor extracellular matrix (ECM), and degrade ECM components.[39] Some studies have suggested that tumor vasodilators can alleviate tumor hypoxia, reverse immunosuppression, and promote tumor invasion, survival, and the directed effector functions of CAR-NK cells.[40] The abnormal development and structural disorganization of tumor vasculature, along with the formation of a high-pressure microenvironment, hinder the recruitment of CAR-NK cells. In our study, we observed that the advanced tongue tumors in mice were compressed by the oral space, which further impaired the blood supply to the tongue and restricted immune cell infiltration. However, after SDT treatment, the tumor volume decreased, relieving compression and improving immune cell recruitment. This may explain why SDT demonstrated better efficacy in nude mice and NSG mice treated with adoptive immunotherapy.

The change in mouse body weight exhibited an inverse correlation with the primary tumor size, as depicted in Figure S18d; the group treated with both SDT and CAR-NK cells experienced the least weight reduction, while the SDT-only and CAR-NK cell-only groups showed significant weight loss, likely due to inadequate inhibition of the primary tumor. Furthermore, no abnormal changes in body temperature were observed in any of the treatment groups (Figure S18c), suggesting that the combination of cancer SDT and immunotherapy is associated with high therapeutic biosafety. Importantly, CAR-NK cell infiltration was not detected in critical organs such as the heart and liver, confirming the safety and high targeting specificity of CAR-NK cell therapy in vivo (Figure S19). Additionally, we analyzed CAR-NK cell infiltration in both local and distant tumors at various treatment stages using flow cytometry (Figure 7b). The results demonstrated that SDT increased CAR-NK cell infiltration in the primary tumor from 3.11 to 21.5%, while infiltration in distant subcutaneous tumors was slightly reduced, consistent with the previous in vivo imaging findings (Figure 6e). These results suggested that SDT enhances immune cell recruitment at the irradiated tumor site, thereby improving the efficacy of the combined SDT and CAR-NK cell therapy.

3. CONCLUSIONS

We designed the HMME@Lip nanosonosensitizer as a substrate to trigger massive ROS generation via noninvasive US, which served as an activation signal for inflammation and induced pyroptosis in OSCC cells. Our results demonstrated that this inflammatory cell death is mediated by Caspase-3 activation, GSDME cleavage, and LDH release, with a marked ability to recruit NK cells. To further enhance this effect, we

https://doi.org/10.1021/acsami.5c03584
ACS Appl. Mater. Interfaces 2025, 17, 29352−29363

engineered CAR-NK cells targeting EGFR-positive cancer cells and validated their antitumor activity in vitro. In an orthotopic OSCC mouse model, we confirmed that SDT improved the tumor-targeting and infiltration abilities of CAR-NK cells, leading to a significantly enhanced therapeutic effect. Given that NK cell immunotherapy has an excellent safety profile with minimal risks of CRS and neurotoxicity, this approach holds promise as an adjunct to various NK cell-based immunotherapies, both in vitro and in vivo. Moreover, the US-triggered nanosonosensitizer-induced pyroptosis exhibited strong antimetastatic potential. Overall, this study introduced a nanomedicine-based strategy to induce pyroptosis-mediated cancer cell death and facilitate NK cell recruitment.

4. EXPERIMENTAL SECTION

Methods for nanomaterials synthesis and characterization, material safety testing, cell culture, in vitro toxicity testing of SDT, RNA sequencing, WB, in vivo imaging, CAR-NK cell construction and its toxicity testing on tumor cells, and SDT combined with CAR-NK treatment of NSG mice are provided in the Supporting Information.

Statistical analysis: All experimental data in this study were measured at least three times and recorded as mean ± SD. Unpaired two-tailed Student's t tests and one-/two-way analysis of variance (ANOVA) were used in this study, depending on the data type. The details can be found in the figure legends including test used, sample size (n), and probability (P) value. $P < 0.05$ was considered to be statistically significant. All the statistical analyses were conducted by GraphPad Prism 9.5 (GraphPad Software, CA, USA). Plots and charts were performed using GraphPad Prism 9.5 and Origin 2021 software (Origin Lab, MA, USA).

■ ASSOCIATED CONTENT

Supporting Information

The Supporting Information is available free of charge at https://pubs.acs.org/doi/10.1021/acsami.5c03584.

Methods for nanomaterial synthesis and characterization, cell culture, in vitro toxicity testing of SDT, RNA sequencing, WB, in vivo imaging, CAR-NK cell construction and its toxicity testing on tumor cells, SDT combined with CAR-NK treatment of NSG mice, relative cell viability, unsupervised hierarchical clustering, calcein-AM staining, H&E staining, and protein sequences

■ AUTHOR INFORMATION

Corresponding Author

Ping Xiong − *Department of Ultrasound, Ninth People's Hospital, Shanghai Jiaotong University School of Medicine, Shanghai 200001, P.R. China;* orcid.org/0000-0002-8755-6815; Email: xiongpxp@163.com

Authors

Jing Meng − *Department of Ultrasound, Ninth People's Hospital, Shanghai Jiaotong University School of Medicine, Shanghai 200001, P.R. China*

Jiaxin Zuo − *Department of Ultrasound, Ninth People's Hospital, Shanghai Jiaotong University School of Medicine, Shanghai 200001, P.R. China*

Luyu Li − *Shanghai Ninth People's Hospital Affiliated to Shanghai Jiao Tong University School of Medicine, Shanghai 200240, China*

Yunxuan Zhang − *School of Pharmacy, Shanghai Jiao Tong University, Shanghai 200240, P.R. China*

Minghao Zhao − *School of Pharmacy, Shanghai Jiao Tong University, Shanghai 200240, P.R. China*

Complete contact information is available at: https://pubs.acs.org/10.1021/acsami.5c03584

Author Contributions

J.M., J.Z., and L.L. contributed equally to this work. J.M. synthesized and characterized the nanosonosensitizers, conducted in vitro and in vivo experiments, and analyzed the data. J.M. wrote the paper. J.Z. supervised the project and commented on the project. L.L. analyzed the RNA sequencing results, created the figures, and wrote the manuscript for the corresponding sections. Y.Z. and M.Z. collected the data and commented on the project. P.X. was responsible for the project conception, supervision, funding acquisition, as well as writing and editing. All authors contributed to the discussion throughout the project.

Funding

The authors greatly acknowledge the financial support from the Shanghai Municipal Commission of Science and Technology [23ZR143800]; the National Natural Science Foundation of China [81971618]; the Shanghai Ninth People's Hospital, the Shanghai Jiao Tong University School of Medicine (N0.JYJC202132), and the Subject Group Construction Project of the Ninth People's Hospital Affiliated to Shanghai Jiao Tong University School of Medicine.

Notes

The ethical review board of Shanghai JiaoTong University School of Medicine, China, approved the animal experiment protocol and strictly followed its guidelines (Ethical approval number: SH9H-2024-A1353-1).

The authors declare no competing financial interest.

■ REFERENCES

(1) Chow, L. Q. M. Head and Neck Cancer. *N Engl J. Med.* **2020**, *382* (1), 60−72.

(2) Galmiche, A.; Saidak, Z.; Bouaoud, J.; Mirghani, H.; Page, C.; Dakpé, S.; Clatot, F. Genomics and precision surgery for head and neck squamous cell carcinoma. *Cancer Lett.* **2020**, *481*, 45−54.

(3) Miyauchi, S.; Kim, S. S.; Pang, J.; Gold, K. A.; Gutkind, J. S.; Califano, J. A.; Mell, L. K.; Cohen, E. E. W.; Sharabi, A. B. Immune Modulation of Head and Neck Squamous Cell Carcinoma and the Tumor Microenvironment by Conventional Therapeutics. *Clin. Cancer Res.* **2019**, *25* (14), 4211−4223.

(4) Johnson, D. E.; Burtness, B.; Leemans, C. R.; Lui, V. W. Y.; Bauman, J. E.; Grandis, J. R. Head and neck squamous cell carcinoma. *Nat. Rev. Dis Primers.* **2020**, *6* (1), 92.

(5) Yue, W.; Chen, L.; Yu, L.; Zhou, B.; Yin, H.; Ren, W.; Liu, C.; Guo, L.; Zhang, Y.; Sun, L.; et al. Checkpoint blockade and nanosonosensitizer-augmented noninvasive sonodynamic therapy combination reduces tumour growth and metastases in mice. *Nat. Commun.* **2019**, *10* (1), 2025.

(6) Xie, G.; Dong, H.; Liang, Y.; Ham, J. D.; Rizwan, R.; Chen, J. CAR-NK cells: A promising cellular immunotherapy for cancer. *EBioMedicine.* **2020**, *59*, No. 102975.

(7) Dagher, O. K.; Posey, A. D., Jr. Forks in the road for CAR T and CAR NK cell cancer therapies. *Nat. Immunol* **2023**, *24* (12), 1994−2007.

(8) Suck, G.; Odendahl, M.; Nowakowska, P.; Seidl, C.; Wels, W. S.; Klingemann, H. G.; Tonn, T. NK-92: an 'off-the-shelf therapeutic' for adoptive natural killer cell-based cancer immunotherapy. *Cancer Immunol Immunother.* **2016**, *65* (4), 485−492.

(9) Qu, C.; Zhang, H.; Cao, H.; Tang, L.; Mo, H.; Liu, F.; Zhang, L.; Yi, Z.; Long, L.; Yan, L.; et al. Tumor buster - where will the CAR-T cell therapy 'missile' go? *Mol. Cancer.* **2022**, *21* (1), 201.

(10) Wolf, N. K.; Kissiov, D. U.; Raulet, D. H. Roles of natural killer cells in immunity to cancer, and applications to immunotherapy. *Nat. Rev. Immunol.* **2023**, *23* (2), 90−105.
(11) Jia, H.; Yang, H.; Xiong, H.; Luo, K. Q. NK cell exhaustion in the tumor microenvironment. *Front Immunol.* **2023**, *14*, No. 1303605.
(12) Althaus, J.; Nilius-Eliliwi, V.; Maghnouj, A.; Döring, S.; Schroers, R.; Hudecek, M.; Hahn, S. A.; Mika, T. Cytotoxicity of CD19-CAR-NK92 cells is primarily mediated via perforin/granzyme pathway. *Cancer Immunol Immunother.* **2023**, *72* (8), 2573−2583.
(13) Gong, L.; Li, Y.; Cui, K.; Chen, Y.; Hong, H.; Li, J.; Li, D.; Yin, Y.; Wu, Z.; Huang, Z. Nanobody-Engineered Natural Killer Cell Conjugates for Solid Tumor Adoptive Immunotherapy. *Small.* **2021**, *17* (45), No. e2103463.
(14) Cifaldi, L.; Locatelli, F.; Marasco, E.; Moretta, L.; Pistoia, V. Boosting Natural Killer Cell-Based Immunotherapy with Anticancer Drugs: a Perspective. *Trends Mol. Med.* **2017**, *23* (12), 1156−1175.
(15) Um, W.; Kumar, E. K. P.; Lee, J.; Kim, C. H.; You, D. G.; Park, J. H. Recent advances in nanomaterial-based augmented sonodynamic therapy of cancer. *Chem. Commun. (Camb)* **2021**, *57* (23), 2854−2866.
(16) Son, S.; Kim, J. H.; Wang, X.; Zhang, C.; Yoon, S. A.; Shin, J.; Sharma, A.; Lee, M. H.; Cheng, L.; Wu, J.; Kim, J. S. Multifunctional sonosensitizers in sonodynamic cancer therapy. *Chem. Soc. Rev.* **2020**, *49* (11), 3244−3261.
(17) Zhao, J.; Duan, L.; Wang, A.; Fei, J.; Li, J. Insight into the efficiency of oxygen introduced photodynamic therapy (PDT) and deep PDT against cancers with various assembled nanocarriers. *Wiley Interdiscip Rev. Nanomed Nanobiotechnol.* **2020**, *12* (1), No. e1583.
(18) Guo, J.; Pan, X.; Wang, C.; Liu, H. Molecular Imaging-Guided Sonodynamic Therapy. *Bioconjug Chem.* **2022**, *33* (6), 993−1010.
(19) Xu, K.; Chang, M.; Wang, Z.; Yang, H.; Jia, Y.; Xu, W.; Zhao, B.; Chen, Y.; Yao, F. Multienzyme-Mimicking LaCoO(3) Nanotrigger for Programming Cancer-Cell Pyroptosis. *Adv. Mater.* **2023**, *35* (35), No. e2302961.
(20) Wang, Y.; Gao, W.; Shi, X.; Ding, J.; Liu, W.; He, H.; Wang, K.; Shao, F. Chemotherapy drugs induce pyroptosis through caspase-3 cleavage of a gasdermin. *Nature.* **2017**, *547* (7661), 99−103.
(21) Luo, Y.; Guan, B.; Deng, X.; Bai, P.; Huang, H.; Miao, C.; Sun, A.; Li, Z.; Yang, D.; Wang, X.; et al. Methuosis Inducer SGI-1027 Cooperates with Everolimus to Promote Apoptosis and Pyroptosis by Triggering Lysosomal Membrane Permeability in Renal Cancer. *Adv. Sci. (Weinh).* **2024**, *11* (38), No. e2404693.
(22) Zhong, H.; Chen, G.; Li, T.; Huang, J.; Lin, M.; Li, B.; Xiao, Z.; Shuai, X. Nanodrug Augmenting Antitumor Immunity for Enhanced TNBC Therapy via Pyroptosis and cGAS-STING Activation. *Nano Lett.* **2023**, *23* (11), 5083−5091.
(23) Kyrysyuk, O.; Wucherpfennig, K. W. Designing Cancer Immunotherapies That Engage T Cells and NK Cells. *Annu. Rev. Immunol.* **2023**, *41*, 17−38.
(24) Wei, X.; Xie, F.; Zhou, X.; Wu, Y.; Yan, H.; Liu, T.; Huang, J.; Wang, F.; Zhou, F.; Zhang, L. Role of pyroptosis in inflammation and cancer. *Cell Mol. Immunol.* **2022**, *19* (9), 971−992.
(25) Broz, P.; Pelegrín, P.; Shao, F. The gasdermins, a protein family executing cell death and inflammation. *Nat. Rev. Immunol.* **2020**, *20* (3), 143−157.
(26) Ye, Y.; Ren, K.; Dong, Y.; Yang, L.; Zhang, D.; Yuan, Z.; Ma, N.; Song, Y.; Huang, X.; Qiao, H. Mitochondria-Targeting Pyroptosis Amplifier of Lonidamine-Modified Black Phosphorus Nanosheets for Glioblastoma Treatments. *ACS Appl. Mater. Interfaces.* **2023**, *15* (22), 26285−26297.
(27) Wang, S.; Zhang, M. J.; Wu, Z. Z.; Zhu, S. W.; Wan, S. C.; Zhang, B. X.; Yang, Q. C.; Xiao, Y.; Chen, L.; Sun, Z. J. GSDME Is Related to Prognosis and Response to Chemotherapy in Oral Cancer. *J. Dent Res.* **2022**, *101* (7), 848−858.
(28) Zhang, J.; Shi, M.; Sun, J.; Xu, L.; Xu, Y.; Jiang, W.; Zhao, W.; Zhou, M.; Mao, C.; Zhang, S. Biodegradable Vanadium-Based Nanomaterials for Photothermal-Enhanced Tumor Ferroptosis and Pyroptosis. *ACS Appl. Mater. Interfaces.* **2025**, *17* (4), 5735−5751.
(29) Zhang, N.; Zeng, W.; Xu, Y.; Li, R.; Wang, M.; Liu, Y.; Qu, S.; Ferrara, K. W.; Dai, Z. Pyroptosis Induction with Nanosonosensitizer-Augmented Sonodynamic Therapy Combined with PD-L1 Blockade Boosts Efficacy against Liver Cancer. *Adv. Healthc Mater.* **2024**, *13* (7), No. e2302606.
(30) Klingemann, H. The NK-92 cell line-30 years later: its impact on natural killer cell research and treatment of cancer. *Cytotherapy.* **2023**, *25* (5), 451−457.
(31) Voldborg, B. R.; Damstrup, L.; Spang-Thomsen, M.; Poulsen, H. S. Epidermal growth factor receptor (EGFR) and EGFR mutations, function and possible role in clinical trials. *Ann. Oncol.* **1997**, *8* (12), 1197−1206.
(32) Spellerberg, R.; Benli-Hoppe, T.; Kitzberger, C.; Hageneier, M.; Schwenk, N.; Öztürk, Ö.; Steiger, K.; Multhoff, G.; Eiber, M.; Schilling, F.; et al. Dual EGFR- and TfR-targeted gene transfer for sodium iodide symporter gene therapy of glioblastoma. *Mol. Ther Oncolytics.* **2022**, *27*, 272−287.
(33) Schönfeld, K.; Sahm, C.; Zhang, C.; Naundorf, S.; Brendel, C.; Odendahl, M.; Nowakowska, P.; Bönig, H.; Köhl, U.; Kloess, S.; et al. Selective inhibition of tumor growth by clonal NK cells expressing an ErbB2/HER2-specific chimeric antigen receptor. *Mol. Ther.* **2015**, *23* (2), 330−338.
(34) Biller, L. H.; Schrag, D. Diagnosis and Treatment of Metastatic Colorectal Cancer: A Review. *Jama.* **2021**, *325* (7), 669−685.
(35) Han, J.; Chu, J.; Keung Chan, W.; Zhang, J.; Wang, Y.; Cohen, J. B.; Victor, A.; Meisen, W. H.; Kim, S. H.; Grandi, P.; et al. CAR-Engineered NK Cells Targeting Wild-Type EGFR and EGFRvIII Enhance Killing of Glioblastoma and Patient-Derived Glioblastoma Stem Cells. *Sci. Rep.* **2015**, *5*, No. 11483.
(36) Richardson, K. C.; Jung, K.; Matsubara, J. A.; Choy, J. C.; Granville, D. J. Granzyme B in aging and age-related pathologies. *Trends Mol. Med.* **2024**, *30* (12), 1165−1179.
(37) Zhang, Z.; Zhang, Y.; Xia, S.; Kong, Q.; Li, S.; Liu, X.; Junqueira, C.; Meza-Sosa, K. F.; Mok, T. M. Y.; Ansara, J.; et al. Gasdermin E suppresses tumour growth by activating anti-tumour immunity. *Nature.* **2020**, *579* (7799), 415−420.
(38) Wang, W.; Zou, R.; Qiu, Y.; Liu, J.; Xin, Y.; He, T.; Qiu, Z. Interaction Networks Converging on Immunosuppressive Roles of Granzyme B: Special Niches Within the Tumor Microenvironment. *Front Immunol.* **2021**, *12*, No. 670324.
(39) Ran, G. H.; Lin, Y. Q.; Tian, L.; Zhang, T.; Yan, D. M.; Yu, J. H.; Deng, Y. C. Natural killer cell homing and trafficking in tissues and tumors: from biology to application. *Signal Transduct Target Ther.* **2022**, *7* (1), 205.
(40) Liu, Y.; Hao, Y.; Chen, J.; Chen, M.; Tian, J.; Lv, X.; Zhang, Y.; Ma, X.; Zhou, Y.; Feng, L. An Injectable Puerarin Depot Can Potentiate Chimeric Antigen Receptor Natural Killer Cell Immunotherapy Against Targeted Solid Tumors by Reversing Tumor Immunosuppression. *Small.* **2024**, *20* (25), No. e2307521.

https://doi.org/10.1021/acsami.5c03584
ACS Appl. Mater. Interfaces 2025, 17, 29352−29363